JPCBFK

MARCH 21, 2019
VOLUME 123
NUMBER 11

pubs.acs.org/JPCB

THE JOURNAL OF PHYSICAL CHEMISTRY B

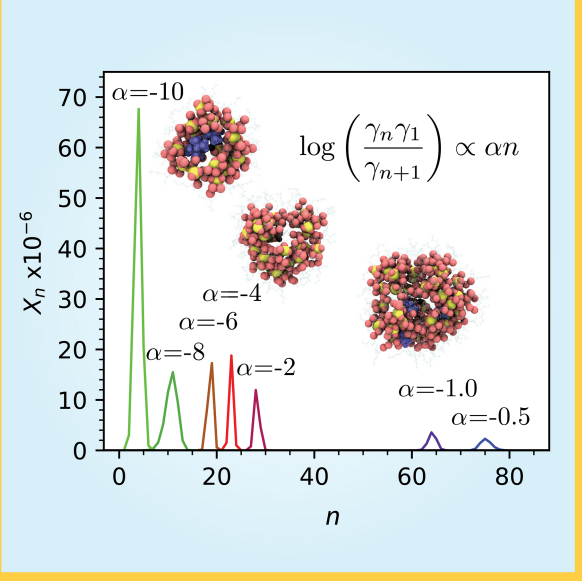

ACS Publications
Most Trusted. Most Cited. Most Read.

www.acs.org

THE JOURNAL OF PHYSICAL CHEMISTRY B

Article

Cite This: J. Phys. Chem. B 2019, 123, 2546−2557

pubs.acs.org/JPCB

Aerosol-OT Surfactant Forms Stable Reverse Micelles in Apolar Solvent in the Absence of Water

Ryo Urano, George A. Pantelopulos, and John E. Straub*

Chemistry Department, Boston University, 590 Commonwealth Avenue, Boston, Massachusetts 02215, United States

ABSTRACT: Normal micelle aggregates of amphiphilic surfactant in aqueous solvents are formed by a process of entropically driven self-assembly. The self-assembly of reverse micelles from amphiphilic surfactant in a nonpolar solvent in the presence of water is considered to be an enthalpically driven process. Although the formation of normal and reverse surfactant micelles has been well characterized in theory and experiment, the nature of dry micelle formation, from amphiphilic surfactant in a nonpolar solvent in the absence of water, is poorly understood. In this study, a theory of dry reverse micelle formation is developed. Variation in free energy during micelle assembly is derived for the specific case of aerosol-OT surfactant in isooctane solvent using atomistic molecular dynamics simulation analyzed using the energy representation method. The existence and thermodynamic stability of dry reverse micelles of limited size are confirmed. The abrupt occurrence of monodisperse aggregates is a clear signature of a critical micelle concentration, commonly observed in the formation of normal surfactant micelles. The morphology of large dry micelles provides insight into the nature of the thermodynamic driving forces stabilizing the formation of the surfactant aggregates. Overall, this study provides detailed insight into the structure and stability of dry reverse micelles assembly in a nonpolar solvent.

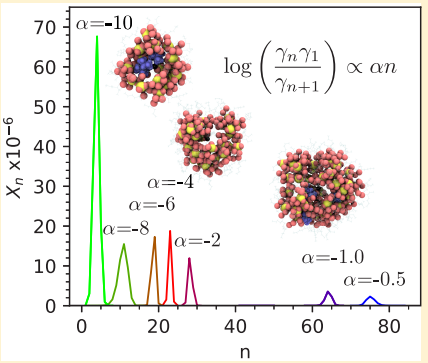

INTRODUCTION

The rich phase behavior and complex dynamics of surfactant microemulsions have been a focus of intense experimental, theoretical, and computational study for decades. The detailed dynamic and thermodynamic behaviors of ternary mixtures of surfactant, oil, and water are fundamentally important to the theory of complex solutions. In addition, self-assembled structures such as micelles, reverse micelles (RMs), and membranes have great applied importance to biology as well as environmental and industrial chemistry. As such, the development of a fundamental understanding of the equilibrium state of microemulsions has been a critical goal for the field.

The RM morphology has been exploited for a variety of applications, including chemical synthesis,[1] drug delivery systems,[2−4] studies of model membranes,[5] and solute encapsulation.[6,7] The reverse micelle (RM) is a phase of particular interest, in which surfactant aggregates containing a water core are suspended in a nonpolar solvent. Surfactants in oil-rich solvent systems are important to industrial products such as pigments[8,9] and dry cleaning detergents.[10]

Although an empirical approach to the optimization of surfactant mixtures has led to a significant advancement, it has proven difficult to physically characterize RM solutions in terms of the distribution of aggregate size and nature of RM structure. As such, there is a pressing need to develop a first-principles theory for the de novo prediction of the RM size distribution as a function of solution composition.

The assembly of normal surfactant micelle in aqueous solvents has long been assumed to be driven by an increase in water entropy following surfactant aggregation and exclusion of water from the micelle interior, leading to favorable changes in entropy and enthalpy upon micelle assembly.[11−17] The assembly of "wet" RMs from mixtures of surfactants, oils, and water in ambient conditions is typically considered to be enthalpy driven, with the RM phase stabilized by favorable interaction of water and surfactant head groups,[18] with size distributions determined by water loading[19] and salt content[20] attributed to electrostatic interactions.[21,22] Micelles generally assemble only once a critical point in the surfactant concentration has been surpassed, commonly known as the "critical micelle concentration" (CMC), at which a delicate enthalpy−entropy balance is struck. The unique aqueous environment experienced by molecules encapsulated in RMs[23−25] has been utilized in molecular synthesis[26] and the study of protein structure.[27,28] In contrast, clear identification of the principal driving force underlying the formation of "dry" RMs from surfactant in oil solvent in the absence of water has remained elusive.[29] As such, the mechanism of surfactant aggregation in oil solvent in the absence of water and the very existence of dry RMs (hereafter referred to as dRMs) continues to be debated.

In early theoretical work, Ruckenstein and Nagarajan[30] used a free energy functional approach for aerosol-OT (AOT) surfactant in a nonpolar solvent to argue that interactions between surfactant head groups and tails create a free energy minimum associated with the stable formation of dRMs.

Received: August 14, 2018
Revised: January 25, 2019
Published: January 28, 2019

DOI: 10.1021/acs.jpcb.8b07847
J. Phys. Chem. B 2019, 123, 2546−2557

Ruckenstein and Nagarajan predicted dRMs to have an "aggregation number" (number of AOT surfactant molecules in a given micelle) of less than 10, suggesting the absence of a CMC. Given this prediction, it has been suggested that the experimentally observed critical micelle concentration in dRM mixtures must result from the presence of trace water molecules (carried over from AOT synthesis and incomplete surfactant "drying") at a ratio of less than one water per AOT molecule. Motivated by experiments[31] suggesting an inverse hexagonal structure in pure sodium AOT solutions, Harrowell et al.[32] investigated the structure of dRMs in sodium sulfate ion clusters in the vacuum state. By considering the observed sodium sulfate ion cluster structure and the structure of AOT reverse micelles as a perturbation of the crystal structure, they obtained a mean aggregation number that was macroscopically large, suggesting that AOT is insoluble in oil solvent.

A variety of experimental studies have confirmed the existence of dry AOT aggregates. Calorimetric studies[33−35] suggest that the stabilizing interaction energy between AOT molecules in organic solvents is so low as to make the formation of AOT oligomers improbable. In contrast, neutron scattering[36] and absorption spectroscopy[37] studies support the existence of a critical micelle concentration. In addition, a variety of studies have led to independent assessments of mean dRM size (the mean number, $\overline{n}$, of surfactants in dRMs), including $\overline{n}$ = 18 by vapor pressure experiments[38] and $\overline{n}$ = 39 and 56 by light scattering.[39,40] More recent small-angle neutron scattering studies[41,42] have shown a sharp transition in the mean dRM size as a function of AOT concentration in nonpolar solvents. Taken together, these experimental studies provide clear support for the existence of a CMC related to dRM formation at higher AOT concentrations. Interestingly, these studies also demonstrate that the dRM size distribution sensitively depends on solvent properties, such as dielectric constant and surfactant solubility.[43]

Significant theoretical work has been done to define the size distribution of surfactant micelles in aqueous solvents. Christopher and Oxtoby[44] proposed a density functional model that assessed free energy contributions to the aggregation process, obtaining a size distribution from numerical minimization of the free energy. Mohan and Kopelevich[45] obtained kinetic rate constant for the formation of spherical micelles formed by nonionic surfactants using a coarse-grained model and kinetic analysis. Kindt and co-workers[46] employed the chemical species model[47] and a statistical dynamical equation for the size distribution parameterized with an equilibrium constant obtained from molecular simulation. Kinoshita and Sugai[48,49] also employed the chemical species model but used the reference interaction site model theory in their simulations to obtain the chemical potential for surfactant aggregates of varying size. Additionally, Kindt and co-workers have expanded on this work to create the partition-enabled analysis of cluster histograms method via novel application of number theory to evaluation of changes in partition function in the chemical species model, enabling rapid and precise refinement of measured reaction rates between n-mers in solutions at equilibrium. In an impressive theoretical study of the equilibrium properties of micelle formation, Yoshii, Okazaki, and others[50−53] employed the chemical species model to obtain a thermodynamic relation defining micelle size in terms of the free energy of surfactant insertions. Their work employed thermodynamic integration (TI) at infinite dilution and surfactant activity coefficients proposed via fitting of experimental data using the Debye−Hückel theory, resulting in a de novo theoretical prediction of the CMC and distribution of micelle size as a function of surfactant concentration.

In this work, we extend the seminal work of Yoshii and Okazaki to study the size distribution of aggregates of AOT in pure isooctane solvent. To address the inherent complexity of the dRM system, the chemical potential for growth of dRMs is evaluated using the classical free energy functional-based energy representation (ER) method.[54−56] The ER method is shown to dramatically increase the efficiency of free energy calculation within sufficient accuracy to provide thermodynamically relevant results. The resulting theory provides a de novo prediction of the surfactant aggregate size distribution, providing evidence for the existence of stable dry AOT RMs and surprising insight into the RM structure and stability.

This paper is organized as follows. In the Methods section, we derive a thermodynamic relation for the relative stability of AOT aggregates as a function of aggregate size. The theoretical foundation for the evaluation of the chemical potential as a function of aggregate size based on our free energy calculations is described in detail. In the Results section, we first determine the free energy of dRM growth by addition of solvated surfactant monomers using the energy representation method. Subsequently, the structures and relative free energies of AOT dRMs are characterized as a function of aggregation number, n. The mean size, $\overline{n}$, is derived and is discussed in terms of the dRM structures observed at each size. Finally, the theoretical results are used to address discrepancies between prior theoretical predictions and experimental observations. Overall, this study provides the first detailed atomic level characterization of the equilibrium distribution of dry AOT reverse micelles.

METHODS

Thermodynamic Relations of Surfactant Size Distributions. The theoretical foundation of our approach is a definition relating the relative concentration of a dry reverse micelle (dRM) of a given size to the activity coefficients and relative free energy differences between dRMs of varying sizes. The starting point is the previous works of Okazaki and co-workers exploring the thermodynamic properties of surfactant micelles.[50−53]

The chemical species model is employed[44,46,48,57−59] in which the composition of the solution is defined in terms of a distribution of dRMs of varying size treating each size as a distinct chemical species. The chemical potential μ_n of an aggregate composed of n surfactant monomers, nA, is written

$$\mu_n = \mu_n^0 + k_B T \ln a_n \tag{1}$$

where μ_n^0 is the chemical potential of a dRM of aggregation number n at a standard state and a_n is the relative activity of a micelle of aggregation number n in the solution at a certain dilution. The standard state is a solvated monomer at infinite dilution, as it is often defined for liquid phase solutes.

The free energy change accompanied by the formation of a dRM of n solutes in the solution, $R_n^{(sol)}$, from n isolated surfactant molecules in a vacuum and a pure solvent system is described by

$$nA^{(vac)} \overset{\mu_n^0}{\rightleftharpoons} R_n^{(sol)} \tag{2}$$

For solvent molecules, the chemical potential, μ_s, is defined as

DOI: 10.1021/acs.jpcb.8b07847
J. Phys. Chem. B 2019, 123, 2546−2557

$$\mu_s = \mu_s^0 + k_B T \ln a_s \tag{3}$$

in terms of the standard state chemical potential μ_s^0 of the solvent and the corresponding activity coefficient, a_s. The total free energy of a solution containing dRMs of various sizes, G, can be written

$$G = N_s\mu_s + \sum_n N_n\mu_n \tag{4}$$

$$= N_s\mu_s^0 + \sum_n \mu_n^0 + k_B T\left(N_s \ln a_s + \sum_n N_n \ln a_n\right) \tag{5}$$

where N_n is the number of each size of dRM and N_s is the total number of solvent molecules.

For the association reaction adding one amphiphilic surfactant molecule to an aggregate of n surfactant molecules in the solution

$$R_n^{(sol)} + A^{(sol)} \overset{\Delta G_{n+1}}{\rightleftharpoons} R_{n+1}^{(sol)} \tag{6}$$

the change in free energy is the difference in chemical potentials for insertion of $n + 1$ from n and 1 monomers from vacuum to form dRMs in the solution described in eq 2. We decompose these chemical potentials to standard state contributions, μ^0, and contributions from the activity (describing extra-micellar interactions), μ^a, as

$$\Delta G_{n+1} = \mu_{n+1} - (\mu_n + \mu_1) \tag{7}$$

$$= (\mu_{n+1}^0 + \mu_{n+1}^a) - (\mu_n^0 + \mu_n^a) - (\mu_1^0 + \mu_1^a) \tag{8}$$

$$= \Delta\mu_{n+1}^0 + k_B T \ln \frac{X_{n+1}}{X_n X_1} + k_B T \ln \frac{\gamma_{n+1}}{\gamma_n \gamma_1} \tag{9}$$

where the difference in chemical potential for adding one surfactant to a pre-existing dRM of aggregation number n at a standard state is

$$\Delta\mu_{n+1}^0 \equiv \mu_{n+1}^0 - (\mu_n^0 + \mu_1^0) \tag{10}$$

The activity coefficient a_n is defined in terms of the mole fraction X_n and activity coefficient γ_n at size n as $a_n = \gamma_n X_n$. At equilibrium $\Delta G_{n+1} = 0$, for which we obtain the final relation defining the dRM size distribution

$$\frac{X_{n+1}}{X_n} = \frac{\gamma_n\gamma_1}{\gamma_{n+1}} X_1 \exp\left(\frac{-\Delta\mu_{n+1}^0}{k_B T}\right) \tag{11}$$

where X_n is the mole fraction of reverse micelles of aggregation number n and $\Delta\mu_{n+1}^0$ is the change in chemical potential associated with the reaction in eq 6 taken to be at a standard state (infinite dilution).

Additionally, the effect of molecular indistinguishability may need to be accounted for in practice, depending on the method used to determine ΔG_{n+1}. Kindt has proposed a correction to account for molecular distinguishability.[60] For the reaction described by ΔG_{n+1}

$$R_n^{(sol)} + A^{(sol)} \underset{k_2}{\overset{k_1}{\rightleftharpoons}} R_{n+1}^{(sol)} \tag{12}$$

the forward rate, k_1, involves only one molecule, A. However, the backward rate, k_2, involves the $n + 1$ indistinguishable members of $R_{n+1}^{(sol)}$. From $R_{n+1}^{(sol)}$, one of the $n + 1$ indistinguishable AOTs will disassociate, leaving an AOT n-mer. Accounting for this will slightly change the free energy such that

$$\Delta G_{n+1}^{corrected} = \Delta G_{n+1} + k_B T \ln(n + 1) \tag{13}$$

This correction scales as $\ln(n)$ and may be considered negligible in many cases when thinking of free energy changes over small ranges of n beyond $n = 10$. As such, this correction does not change the qualitative results of our study or the past work of Yoshii and co-workers.[50−53] Careful consideration of such reaction rates may need to be considered depending on the study and methodology employed in future works.

Physical Meaning of Thermodynamic Quantities. To obtain the size distribution of RMs according to eq 11, it is necessary to determine the aforementioned chemical potential difference at infinite dilution $\Delta\mu_{n+1}^0$ and activity coefficient γ_n for all physically relevant values of n. The activity coefficient γ_n is often derived from fitting experimental solvation data to the predictions of the Debye−Hückel theory.

Consider the insertion of a surfactant molecule into a dRM of given aggregation number n leading to the formation of a dRM of aggregation number $n + 1$. The ratio of concentrations of the two species can be related to the change in free energy upon surfactant molecule insertion as

$$\frac{X_n}{X_1} = \left(\frac{\gamma_1}{\gamma_n}\right)(\gamma_1 X_1)^{n-1} \exp\left(\frac{[\sum_{i=2}^{n} -\Delta\mu_i^0]}{k_B T}\right) \text{ for } n \geq 2 \tag{14}$$

Having computed the dRM size distribution in terms of the concentrations of dRM sizes, the law of mass action can be used to relate the relative concentrations of dRMs to the solute concentration of surfactant as

$$\sum_n nX_n = N_{AOT}/N_{ISO} \tag{15}$$

Relative Free Energy Evaluation. To determine the free energy change upon insertion of a surfactant molecule into a pre-existing dRM, we employ the energy representation (ER) method.[54−56] We briefly introduce the formally exact free energy evaluation method of thermodynamic integration (TI) followed by a discussion of the approximate ER method (ER).

Following the notation of Frolov,[61] the potential energy function of the solute−solvent system is written

$$V(\mathbf{r}_s, \mathbf{r}_w) = \Phi(\mathbf{r}_w) + v(\mathbf{r}_s, \mathbf{r}_w) \tag{16}$$

consisting of the solvent−solvent potential $\Phi(\mathbf{r}_w)$ and full coupling solute−solvent potential $v(\mathbf{r}_s, \mathbf{r}_w)$, where $\mathbf{r}_s$ represents the configuration of the solute molecule and $\mathbf{r}_w$ the configuration of the solvent molecules. We assume that the λ-dependent solute−solvent interaction is linearly modulated by parameter λ as

$$V(\mathbf{r}_s, \mathbf{r}_w; \lambda) = \Phi(\mathbf{r}_w) + u_\lambda(\mathbf{r}_s, \mathbf{r}_w) = \Phi(\mathbf{r}_w) + \lambda v(\mathbf{r}_s, \mathbf{r}_w) \tag{17}$$

where $\lambda = 0$ represents the pure solvent system $V(\mathbf{r}_s, \mathbf{r}_w; \lambda = 0) = \Phi(\mathbf{r}_w)$ and $\lambda = 1$ represents the full interaction between solute and solvent $V(\mathbf{r}_s, \mathbf{r}_w; \lambda = 1) = \Phi(\mathbf{r}_w) + v(\mathbf{r}_s, \mathbf{r}_w)$.

Thermodynamic Integration (TI) Approach. The excess chemical potential (change in solvation free energy) of the solute can be written using Kirkwood's charging formula

DOI: 10.1021/acs.jpcb.8b07847
J. Phys. Chem. B 2019, 123, 2546−2557

$$\mu^{ex} = G_{u_{\lambda=1}}(\mathbf{r}_s, \mathbf{r}_w) - G_{u_{\lambda=0}}(\mathbf{r}_s, \mathbf{r}_w)$$
$$= \int_0^1 d\lambda \int d\mathbf{r}_s\, d\mathbf{r}_w \frac{\partial u_\lambda(\mathbf{r}_s, \mathbf{r}_w)}{\partial\lambda} \rho_\lambda(\mathbf{r}_s, \mathbf{r}_w) = \langle \frac{\partial u_\lambda(\mathbf{r}_s, \mathbf{r}_w)}{\partial\lambda} \rangle_\lambda \quad (18)$$

which forms a popular foundation for thermodynamic integration (TI). The quantity $\rho_\lambda(\mathbf{r}_s, \mathbf{r}_w)$ is the normalized classical density distribution corresponding to a potential energy of interaction given by eq 17 for a particular value of λ. In TI, knowledge of intermediate states between $\lambda = 0$ and 1 is required for evaluation of the λ integral. As such, the ensemble average of $\partial u_\lambda/\partial\lambda$ is required for each value of λ. An effective parameterization of $V(\mathbf{r}_s, \mathbf{r}_w; \lambda)$ and sufficient sampling at intermediate and end states are essential to the success of the TI approach.

Energy Representation (ER) Method. An alternative to the formally exact TI approach is the approximate energy representation (ER) method. In the ER method, integration over configuration space of the solute and solvent is replaced by integration over the interaction energy between solute and solvent. The classical density distribution $\rho_\lambda(\mathbf{r}_s, \mathbf{r}_w)$ is replaced by the probability density of specific values of the interaction potential

$$\rho_{sw,\lambda}(\epsilon) = \sum_{i=1}^{N_w} \delta(v(\mathbf{r}_s, \mathbf{r}_w) - \epsilon) \quad (19)$$

where the energy coordinate is defined as $u_\lambda(\epsilon) = \int_{-\infty}^{\infty} d\mathbf{r}_s\, d\mathbf{r}_w\, \delta(v(\mathbf{r}_s,\mathbf{r}_w) - \epsilon) u_\lambda(\mathbf{r}_s,\mathbf{r}_w)$.

The completeness and equivalence of the energy representation to the phase space representation are supported by the Kohn−Sham density functional theorem. In the ER method, information for parameterizing the energy density is obtained from computer simulation.

The formally exact result for μ^{ex} given by eq 18 may be reformed as

$$\mu^{ex} = \int_0^1 d\lambda \int d\mathbf{r}_s\, d\mathbf{r}_w \frac{\partial u_\lambda(\mathbf{r}_s, \mathbf{r}_w)}{\partial\lambda} \rho_\lambda(\mathbf{r}_s, \mathbf{r}_w)$$
$$= \int_{-\infty}^{\infty} d\epsilon \rho_{sw,\lambda=1}(\epsilon)\epsilon - \int_0^1 d\lambda \int_{-\infty}^{\infty} d\epsilon \frac{\partial\rho_{sw,\lambda}(\epsilon)}{\partial\lambda} u_{sw,\lambda}(\epsilon) \quad (20)$$

where $u_{sw,\lambda=1}(\epsilon) = v_{sw}(\epsilon) = \epsilon$ from the definition of the energy coordinate. The first term corresponds to the solute−solvent interaction energy. To evaluate the second term, we introduce an auxiliary function $\omega_{sw,\lambda}$, which is the analog of the potential of mean force and defined through the relation

$$\rho_{sw,\lambda}(\epsilon) = \rho_{sw,\lambda=0}(\epsilon) \exp[-\beta(u_{sw,\lambda}(\epsilon) + \omega_{sw,\lambda}(\epsilon))] \quad (21)$$

The function $\omega_{sw,\lambda}(\epsilon)$ captures the many-body interaction between solute and solvent.

The energy density is written as the linear combination

$$\rho_{sw,\lambda}(\epsilon) = \lambda\rho_{sw,\lambda=1}(\epsilon) + (1 - \lambda)\rho_{sw,\lambda=0}(\epsilon) \quad (22)$$

and given the potential of mean force and direct interaction energy $u_{sw,\lambda}(\epsilon)$, we can transform the second term in eq 20 as

$$\mathcal{F}[\rho_{sw,\lambda}(\epsilon), u_{sw,\lambda}(\epsilon)] \equiv -\int_0^1 d\lambda \int_{-\infty}^{\infty} d\epsilon \frac{\partial\rho_{sw,\lambda}(\epsilon)}{\partial\lambda} u_{sw,\lambda}(\epsilon) \quad (23)$$

$$= k_B T \int d\epsilon \Bigg[(\rho_{sw,\lambda=1}(\epsilon) - \rho_{sw,\lambda=0}(\epsilon)) - \rho_{sw,\lambda=1}(\epsilon) \ln \frac{\rho_{sw,\lambda=1}(\epsilon)}{\rho_{sw,\lambda=0}(\epsilon)} - \beta(\rho_{sw,\lambda=1}(\epsilon) - \rho_{sw,\lambda=0}(\epsilon)) \int_0^1 d\lambda\, \omega_{sw,\lambda}(\epsilon) \Bigg] \quad (24)$$

where we have used the identity

$$\frac{\partial\rho_{sw,\lambda}(\epsilon)}{\partial\lambda} = \rho_{sw,\lambda=1}(\epsilon) - \rho_{sw,\lambda=0}(\epsilon) \quad (25)$$

Finally, the excess chemical potential in the energy representation can be written

$$\mu^{ex}[\rho_{sw,\lambda}(\epsilon), u_{sw,\lambda}(\epsilon)] = \int_{-\infty}^{\infty} d\epsilon\, \rho_{sw,\lambda=1}(\epsilon)\epsilon - \mathcal{F}[\rho_{sw,\lambda}(\epsilon), u_{sw,\lambda}(\epsilon)] \quad (26)$$

This equation is exact if the potential mean force $\omega_{sw,\lambda}(\epsilon)$ is exact. However, as in all integral equation theories, $\omega_{sw,\lambda}$ must be treated approximately. As such, the accuracy of this method depends on how well the approximate form of the potential of mean force captures many-body interactions that are not included in the direct interaction of solute and solvent.

The pioneering work of Matubayasi and Nakahara provides guidance on the best choice of functional forms for the potential of mean force $\omega(\epsilon)$. Their new form recommends the use of (1) a hypernetted chain (HNC) equation-inspired contribution for $\omega^{(HNC)}(\epsilon) < 0$, capturing attractions, combined with (2) a Percus−Yevick (PY) equation-inspired term for $\omega^{(PY)}(\epsilon) > 0$, capturing repulsions. The sign of $\omega(\epsilon)$ shows the clear boundary between the repulsions and attractions. By exploiting this insight, the λ integral can be heuristically weighed through a function $\alpha(\epsilon)$ as

$$\beta \int_0^1 d\lambda\, \omega_{sw,\lambda}(\epsilon) \approx \alpha(\epsilon) F_{\omega_1}(\epsilon) + (1 - \alpha(\epsilon)) F_{\omega_0}(\epsilon) \quad (27)$$

where $F_{\omega 1}(\epsilon) = \beta\int_0^1 d\lambda\, \omega_{sw,\lambda=1}(\epsilon)$ and $F_{\omega 0}(\epsilon) = \beta\int_0^1 d\lambda\, \omega_{sw,\lambda=0}(\epsilon)$. The specific form of $\alpha(\epsilon)$ is discussed in detail elsewhere.[55,61] In this way, the λ integral required for the determination of the excess chemical potential in the ER method may be evaluated solely based on knowledge of the energy density at the endpoints $\lambda = 1$ and 0 through $\rho_{sw,\lambda=1}(\epsilon)$ and $\rho_{sw,\lambda=0}(\epsilon)$. In this way, the simulation of intermediate states for the system is avoided, providing a distinct advantage over the TI method. However, many-body effects are approximately included. In systems for which many-body interactions are important, the accuracy of this method is expected to diminish.

Application of the ER Method. We employed the ER method to determine $\Delta\mu^0_{n+1}$ (eq 10) to understand the size distribution of AOT dRMs in pure isooctane solvent within a thermodynamically relevant range of n. We chose to investigate dRMs of n = 1, 10, 20, 30, 40, 50, 60, 70, 75, 80, 90, and 100, requiring simulation of each corresponding $n + 1$ dRM for each n dRM. Rather than directly compute the formation of n-mers from vacuum (eq 11), we directly evaluated $\Delta\mu_{n+1}{}^0$ by using the ER method to calculate the free energy of insertion of a monomer in the solution to a n-mer in the solution. To

DOI: 10.1021/acs.jpcb.8b07847
J. Phys. Chem. B 2019, 123, 2546−2557

calculate $\Delta\mu_{n+1}{}^0$, we used the ER method via the ERmod program (version 0.3.4).[62]

For example, $\Delta\mu^0_{10+1}$ was calculated by evaluation of $\Delta\mu^0$ for insertion of an AOT monomer from a dilute solution to a dilute solution of isooctane solvent containing a dRM of 10 AOTs, as illustrated in Figure 1. This was accomplished by

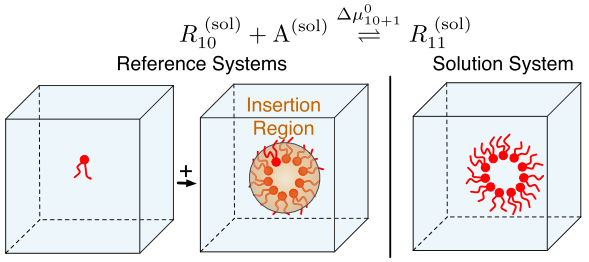

Figure 1. Systems involved in the determination of the free energy of AOT insertion to solvent from vacuum and AOT association of a monomer from solution to a 10-mer. The orange region indicates the ensemble-averaged radius of gyration of the 10-mer, to which solution monomer test insertion centers of mass were constrained.

evaluating the interaction density function via simulation of (1) the "solution" system of an AOT 11-mer in isooctane solvent and (2) the "reference" systems of two independent simulations, one of an AOT 10-mer in isooctane and one of a simulation of an AOT monomer in isooctane. The reference systems were used to evaluate interaction energies of AOT monomer test insertions to the 10-mer solution. Test insertions of AOT monomer centers of mass were constrained to a spherical region described by the radius of gyration (R_g) of the 10-mer dRM, $0 < r < R_g$. Figure 1 describes the simulations needed to determine $\Delta\mu_{10+1}{}^0$.

Test insertions of the solute were performed 10 000 times for each reference configuration. Error bars were computed using the following scheme. (1) Averages were calculated for the solution system with statistical error measured by splitting the trajectory into 10-block subtrajectories. (2) Energy distributions were constructed in which the energy was discretized, respecting a mesh size of $\Delta\epsilon$. The mesh size was increased from a chosen size to that value multiplied by a factor of 1, 2, 3,..., and 10, e.g., $\Delta\epsilon$ = 0.001, 0.002,..., and 0.01 kcal/mol. $\Delta\mu^0$ computed for each mesh size was used as a measure of the mesh size error. Differences in $\Delta\mu^0$ between trajectory blocks using the same mesh size were found to be at most 2.0 kcal/mol for all aggregate sizes. As an example, the composite error of roughly 12 kcal/mol for n = 90 is composed of the statistical error in the trajectory average of 2.0 kcal/mol and the error associated with mesh size dependence of 10 kcal/mol.

System Setup. Initial conditions were defined by spherically arranged configurations of surfactant molecules created using Packmol.[63] Isooctane solvent molecules were arranged surrounding the sphere of AOT, leaving a vacuum in the dRM center. The energy of each system was minimized using the steepest descent algorithm to remove bad contacts. Each system was subsequently equilibrated in the NVT ensemble with velocity rescaling for 300 ps, followed by equilibration in the NPT ensemble with the Nosé–Hoover thermostat and the Parrinello–Rahman barostat for an additional 300 ps. Finally, each system was equilibrated at 300 K and 1 bar to find an average density of approximately 0.7 g/cm^3. Production runs were subsequently performed for 70 ns in the NVT ensemble. In these simulations, the time step was 2 fs using bond length constraints through LINCS for all hydrogens bonded to heavy atoms. Electrostatic calculations were performed using the particle mesh Ewald method with a 1.2 Å cutoff in a rectangular box. The van der Waals term was calculated using a potential switch between 1.0 and 1.2 nm. We employed the modified CHARMM force field developed by Abel and coworkers[64] for AOT surfactant and isooctane solvent molecules. A list of n + 1 systems studied is provided in Table 1 as well as

Table 1. Solution Composition and Average Radius of Gyration (R_g), Asphericity (A_s), and Chemical Potential for Growth to an (n + 1)-mer

N_{AOT}	N_{ISO}	R_g (nm)	A_s	$\Delta\mu^0_{n+1}$ (kcal/mol)
1	3500	N/A	N/A	−13.44 ± 0.47
10	3500	1.04 ± 0.01	0.48 ± 0.002	−55.9 ± 2.4
20	3500	1.17 ± 0.01	0.18 ± 0.001	−89.0 ± 4.4
30	3500	1.31 ± 0.28	0.21 ± 0.001	−78.2 ± 3.7
40	3500	1.47 ± 0.01	0.16 ± 0.008	−85.0 ± 5.3
50	3500	1.58 ± 0.01	0.18 ± 0.001	−84.1 ± 5.1
60	3500	1.67 ± 0.01	0.11 ± 0.001	−95.9 ± 5.9
70	3500	1.79 ± 0.01	0.20 ± 0.001	−93.0 ± 4.5
80	7000	1.78 ± 0.01	0.22 ± 0.001	−90.5 ± 10.3
90	7000	1.97 ± 0.02	0.18 ± 0.001	−91.3 ± 12.6
100	7000	2.07 ± 0.01	0.10 ± 0.001	−85.2 ± 9.3

average radii of gyration and asphericities. Images were rendered using Visual Molecular Dynamics.[65] GROMACS 5.1[66−68] was used to perform system preparation, minimization, and molecular dynamics simulation. Structural and statistical analysis was performed using R.[69−71]

Production simulations of (n + 1)-mer systems were 70 ns length, employing a sampling interval of 10 ps. Production simulations of n-mer reference systems were 70 ns in length and employed a sampling interval of 4 ps. Only the last 50 ns of both of these simulations were used for analysis with ERmod. The structure of the AOT monomer reference system was performed for 70 ns with a sampling of 0.4 ps, and only the last 5 ns of this simulation were used for test insertions.

Following the simulation, we found that dRM aggregates formed irregular, nonspherical shapes. As is often done in studies of micelle structure, we quantified the deviation in dRM shapes from a perfect sphere by calculating the asphericity (A_s) of dRMs in the last 50 ns of all simulated systems. For a RM of total mass, M, the principal moments of inertia, $I_1 > I_2 > I_3$, are related to the semiaxes a, b, c defined as

$$I_1 = \frac{1}{5}M(a^2 + b^2),\ a^2 = \frac{5}{2M}(I_1 + I_2 - I_3) \tag{28}$$

$$I_2 = \frac{1}{5}M(a^2 + c^2),\ b^2 = \frac{5}{2M}(I_1 - I_2 + I_3) \tag{29}$$

$$I_3 = \frac{1}{5}M(b^2 + c^2),\ c^2 = \frac{5}{2M}(-I_1 + I_2 + I_3) \tag{30}$$

For the semiaxes $a > b > c$ of an ellipsoid, A_s is defined

$$A_s = \frac{\lambda_z^2 - \frac{1}{2}(\lambda_x^2 + \lambda_y^2)}{\lambda_{z^2}},\ \lambda_x^2 \le \lambda_y^2 \le \lambda_z^2 \tag{31}$$

where A_s = 0 for a sphere. The radius of gyration R_g is defined as

DOI: 10.1021/acs.jpcb.8b07847
J. Phys. Chem. B 2019, 123, 2546−2557

$$R_g^2 = \frac{\sum_i m_i (r_i - r_{com})^2}{M} = \frac{a^2 + b^2 + c^2}{5} \quad (32)$$

where m_i is the mass of atom i at distance r_i from the RM's center-of-mass, r_{com}. The average radius of the dRM is $(abc)^{1/3}$, corresponding to the radius of a sphere with the same volume.

RESULTS

We characterized AOT aggregates of n-components in isooctane solvent, forming dry reverse micelles (dRM) of size n. The radius of gyration (R_g), asphericity (A_s), and mass distribution functions of these dRMs provide insight into their internal structure. Table 1 lists the compositions of each simulated system, defined by the number of AOT molecules and the overall number of isooctane molecules used in the free energy evaluation. As expected, the R_g increases as n increases, and A_s approaches zero at large n.

A principal result of this study is the determination of the chemical potential at a standard state (infinitely dilute solution) for the process of adding one surfactant, A, to an existing micelle aggregate: R_n, $R_n + A \overset{\Delta\mu^0_{n+1}}{\rightleftharpoons} R_{n+1}$. $\Delta\mu^0_{n+1}$, derived from eq 11, is shown in Figure 2 as a function of aggregate number n. The changes in free energy were computed approximately using the ER method and were interpolated to determine values of the change in the chemical potential for intermediate values of n (see Methods).

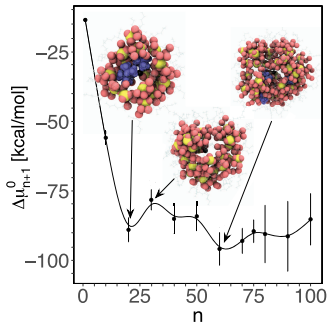

Figure 2. Chemical potential, representing the change in free energy at a standard state for a surfactant molecule to be added to a pre-existing AOT n-mer. Representative structures are shown for n = 20, 30, and 60. The black sphere is the center-of-mass of the aggregate. Oxygen and sulfur atoms of AOT head groups are represented by a CPK model, whereas the aliphatic surfactant tails are represented by lines. The blue molecule in n = 60 is an isooctane molecule confined in the core of the aggregate.

The overall profile of $\Delta\mu^0_{n+1}$ shows a rapid decrease with increasing aggregate size for small n, followed by a minimum near n = 20 and subsequent increase to intermediate values near n = 30. As n increases further, a broad second minimum is identified followed by a plateau for larger n. Insight into the nonmonotonic behavior of the free energy is provided by the representative structures associated with the two minima and intermediate maximum. Clearly, the dry micelle aggregates possess a structure that is not well captured by the radius of gyration and asphericity alone.

Further insight into the structure of aggregates of varying size is provided by analysis of the internal mass density distribution. Figure 3 depicts the mass density of several atom groups as a function of distance from the center-of-mass of the dRM. The mass distributions suggest that the abrupt change in free energy between n = 20 and 30 results from the aggregation of head groups near the center-of-mass of the dry micelle.

In the n = 20 dRM, AOT head groups co-localize near the center-of-mass leading to a peak in the sulfur atom mass distribution near 8 Å, and oxygen and sodium peaks also appear near 8 Å in Figure 3a. As the representative inset structure shows, the head groups form a folded "taco shell" conformation rather than a spherical aggregate. This allows for the formation of a compact micelle structure with head groups packed near the micelle center while minimizing head group repulsion. A few isooctane molecules were found to fill the core of the dRM taco shell rather than near the AOT tails. Such penetration is possible as a result of the small difference in surface tension between organic solvent, 25−35 mN/m,[13,43] and AOT, 30 mN/m.[72] This can be compared to the value for water, 70 mN/m. Given the small difference in surface tension, structural fluctuations that allow the dRM center to have both AOT tail and isooctane solvent are possible. This minimum at n = 20 is a bit larger than that predicted by Eskici and Axelsen, n = 13.6, found by extrapolation of a relation of numbers of water, surfactant, and salt-in spherical RMs from simulations at water loading 7.5 in similarly dilute conditions. Eskici and Axelsen's extrapolation might otherwise hold if we did not observe such complex aggregate shapes in these dry conditions, which allow for a higher degree of AOT aggregation.

The n = 30 dRM is less stable than other slightly larger or smaller dRMs, as $\Delta\mu^0_{30+1}$ is a local maximum in Figure 2. Head group repulsion leads to a more complex dRM structure. Although the overall asphericity of the aggregate is small (0.21), the internal structure associated with the arrangement of surfactant head groups creates two joined tori. This internal structure reflects a mass distribution with a strong peak in AOT tail group density near 5 Å, with a wider sulfur atom

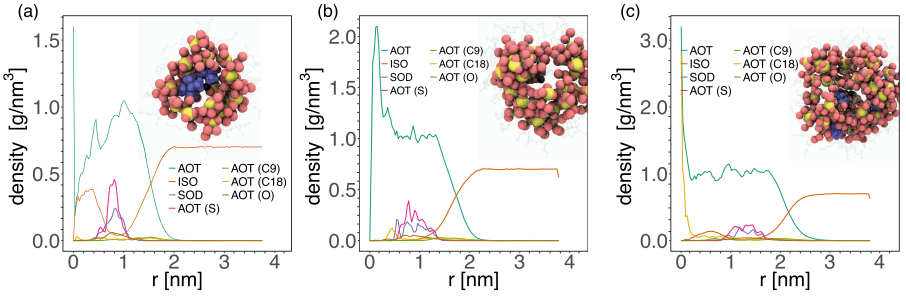

Figure 3. Mass densities of many surfactant components are depicted as a function of distance from the center-of-mass of the dRM for n = (a) 20, (b) 30, and (c) 60. Oxygen and sulfur atoms of AOT head groups are red and yellow, respectively, and aliphatic surfactant tails are transparent gray. The isooctane molecules occupying the dRM core are shown in blue.

DOI: 10.1021/acs.jpcb.8b07847
J. Phys. Chem. B 2019, 123, 2546−2557

distribution between 6 and 12 Å in Figure 3b. This suggests that the shift in the position of the AOT sulfur atoms makes an important contribution to the free energy surface maximum. It seems that the identity of dRM core molecules (isooctane or AOT tails) has little effect on the interaction energy in comparison to the electrostatic energy of surfactant head group interactions.

As the micelle size increases further to $n = 60$, at which point we observe the global minimum in chemical potential, a second morphological transition occurs in Figure 2. A spherical shell of AOT head groups forms, reflected by a peak in the sulfur atom mass density between 14 and 17 Å in Figure 3c. There is a substantial density of surfactant tail groups and isooctane molecules in the center of the micelle, suggesting that the micelle core is composed of nonpolar molecules in contrast to the structure of a wet reverse micelle.

This arrangement of surfactant head groups, distributed over a spherical shell containing surfactant tail groups as well as nonpolar solvent, is reflected in a decrease in $\Delta\mu^0_{n+1}$. After $n = 60$, $\Delta\mu^0_{n+1}$ is observed to plateau at a constant value within the error bars of our computed values.

The observed penetration of nonpolar solvent molecules has been proposed for wet reverse micelles in benzene solvent based on NMR experiments.[73] However, the inclusion of a nonpolar solvent in the core of dry AOT RMs has not been previously observed or proposed. Moreover, the structural fluctuation of solvent molecules after the formation of the micelle is consistent with the unfavorable entropy and enthalpy differences observed in the experiment. In micellization of normal micelles, fluctuations in surfactant molecules decrease, whereas fluctuations in water molecules increase, leading to an increase in entropy during formation. However, in dRM formation, micellization causes surfactant molecules to lose translational entropy, leading to a decrease in total entropy. This provides an explanation for the negative entropy change associated with RM micellization. It appears that the structure of larger dRMs balances the favorable aggregation of surfactant while minimizing the penalty of electrostatic repulsion among charged anionic head groups. Upon reaching a critical size, the dRM is able to form a spherical structure characterized by a shell of head groups with nonpolar surfactant tails facing outward from the dRM center, encapsulating a nonpolar solvent core. This provides an explanation for the long-standing question of how anionic AOT surfactant molecules can form reverse micelle structures in a nonpolar solvent in the absence of a co-surfactant or water.

This work thus far has only considered AOT dRMs in near infinite dilute condition, such that there is no contribution to the chemical activity from intermicellar interactions. Considering the activity coefficients for AOT reverse micelles, we expect that molecular charging will require higher energy cost in nonpolar as opposed to water solvent. In particular, the anionic AOT molecules strongly mediate such charging in a nonpolar solvent,[74,75] and we expect electrostatic interaction among RMs to strongly affect their size distribution. Similar electrostatic interactions have been examined in various experiments and explained in terms of the Debye−Hückel theory and its screened potential form.[76−79] Moreover, the charge fluctuation theory by Eicke et al., which assumes that no electrostatic interaction was found to agree with wet RM experimental data only at relatively higher water concentrations, failing as water concentrations approached dry conditions. Those authors assigned the observed deviation to intermicellar electrostatic interactions in dry conditions,[80] implying that dRMs are charged during micelle−micelle collisions at equilibrium. These past observations in combination with our observation of dRM size and shape (controlled by intra-aggregate electrostatic repulsions) suggest that the Debye−Hückel theory can provide an accurate description of the activity. As such, we assume

$$\log\left(\frac{\gamma_n\gamma_1}{\gamma_{n+1}}\right) \propto \alpha n \tag{33}$$

implying a simple relation between representative charge and aggregate size, $\log\gamma_n \propto \alpha' q^2 = \alpha n^2$ as previously used for normal micelles.[52] We note that there is no molecularly detailed information available for the intermicellar charges felt by dRMs as a function of size. As such, we assume that the charge and size are proportional to each other for simplicity.

With this assumption, α determines how much the charge of dRMs increase as a function of size, which may depend on conditions such as the identity of nonpolar solvents, the ionic strength resulting from head group charges and counter ion type, and temperature. This scaling is expected to be valid in the dilute neutral electrolyte solution for concentration on the order of 0.1 M. To investigate the effect of varying activity coefficient, we explored a range of α, $-\infty < \alpha < 0$ ($0 < \frac{\gamma_n\gamma_1}{\gamma_{n+1}} < 1$). In this range, $\alpha = -\infty$ represents a "salt-out" state where only monomers are formed in the solution (Figure 4a). Somewhere within this range, we expect a value of α which produces a "micellar" solution (Figure 4b), exhibiting a critical micelle concentration near our first local minimum in $\Delta\mu^0_{n+1}$. $\alpha = 0$ represents a "phase-separated" state, where the largest possible dRM is formed from all surfactants in the solution (Figure 4c). Using this, assumed relation allows us to probe the effect of interaggregate interactions for a given size distribution.

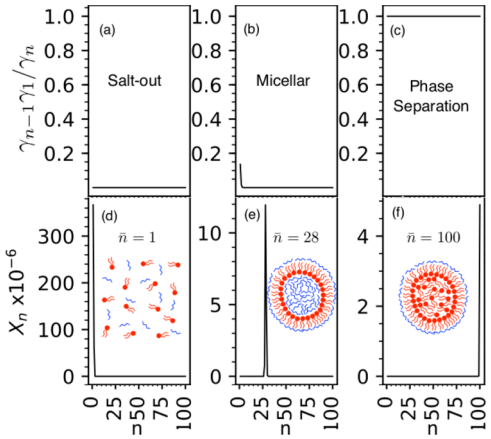

Figure 4. Activity coefficient ratios as a function of n of (a) $\alpha = 0$, (b) $\alpha = -2$, and (c) $\alpha \simeq -\infty$ correspond to salt-out, micellar, and phase-separated dRM solutions in systems containing up to 100 surfactant molecules. Below, the surfactant aggregate number distributions produced by corresponding activity coefficient ratio in (d)−(f). In (f), $\bar{n}$ will be the total of all surfactant molecules in the system, forming a single aggregate. Cartoons depict surfactant (red) and nonpolar solvent (blue).

We rewrite the size distribution given in eq 11 relative to an assumed monomer mole fraction, employ our assumed value

DOI: 10.1021/acs.jpcb.8b07847
J. Phys. Chem. B 2019, 123, 2546−2557

for α, and multiply smaller size relations iteratively transforming eq 11 into

$$\log X_n = n \log X_1 + \alpha \sum_{i=1}^{n-1} i - \frac{\sum_{i=2}^{n} \Delta\mu_i^0}{k_B T} \quad (34)$$

This equation displays how the free energy surface and α determine the mole fraction of aggregates of size n. Using this relation, we demonstrate the values of α that produce the aforementioned salt-out, micellar, and phase-separated distributions of X_n (Figure 4). The salt-out in Figure 4a and phase separated in Figure 4c conditions correspond to $\alpha \simeq -\infty$ and $\alpha = 0$. We discovered that a value of $\alpha = -2$ produces an apparent critical micelle concentration at $\bar{n} = 28$ in Figure 4b. The actual solution of AOT surfactant in isooctane solvent must balance electrostatic repulsions and entropic penalties resulting from the aggregate concentration in the equilibrium state.[74] This implies that larger aggregates have strong electrostatic repulsion, whereas monomer and smaller aggregates are stabilized by entropy. These results suggest that interaction between dRMs is sensitive to AOT surfactant concentration.

To better appreciate the aggregate size distribution depicted in Figure 4b, the balance of each term in eq 34 is shown in Figure 5. α was set to -2, and the total mole fraction was

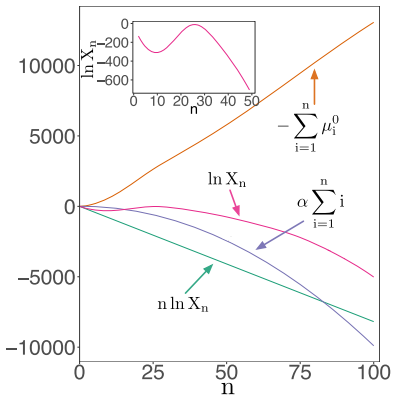

Figure 5. Individual terms contributing to eq 34 as a function of aggregate size. The inset figure shows the expansion of the logarithm of the aggregate mole fraction. α is set to -2. The X_1 value is set such that $c = c^m$.

conserved at the CMC for the X_1 term. These separate contributions show that the finite aggregation at $n = 28$ occurs due to the convex nature of the cumulative sum of free energy from the local minimum at $n = 20$ through the local maximum at $n = 30$. The narrow distribution is a direct reflection of the height of the barrier separating the local minima. The height of the barrier is on the order of several tens of kcal/mol resulting in a relatively monodisperse aggregate size distribution characteristic of a critical micelle concentration.

Rather than imposing a constant α for any total concentration of AOT, as in eq 33, it is more physically meaningful to introduce penalties to the size distribution of dRMs when surfactant concentrations exceed the critical micelle concentration, c^m. A small change in the mean aggregate size at concentrations higher than the CMC has been observed in experiments.[42] This implies that near the CMC, the activity coefficient abruptly increases from near zero as a function of concentration and may subsequently be considered essentially constant. Although normal micelle formation is dominated by the free energy difference between dispersed aggregated states and micelle states, it seems that interactions among dry micelles are a driving force that determines the equilibrium state size distribution. The importance of micelle−micelle interactions for the observed phase transition near the CMC has been previously suggested.[81−84] However, to our knowledge, no previous theory has captured the difference in free energy associated with intermicelle interaction.

As such, we employ an interpolation of α between values representing the salt-in state ($\alpha_{\text{salt-in}}$) and micelle state (α_{micellar}) using a sigmoidal function to reproduce the sudden occurrence of micelles near the CMC as a function of the surfactant concentration ($c = \sum_{n=1} n X_n$) expressed as

$$\alpha(c) = A + \frac{(\alpha_{\text{salt-in}} - \alpha_{\text{micellar}})}{[1 + \exp(-A(c - c^m))]^{(B^{-1})}} \quad (35)$$

where A and B scale the sigmoid form, set to $A = 10^6$ and $B = 35$. We set $\alpha_{\text{salt-in}} = -30$ and $\alpha_{\text{micellar}} = -2$.

Using this interpolated function $\alpha(c)$, we test how various values for the ratio of CMC (c^m) to surfactant concentration (c) control the size distribution. Figure 6 shows the micelle size

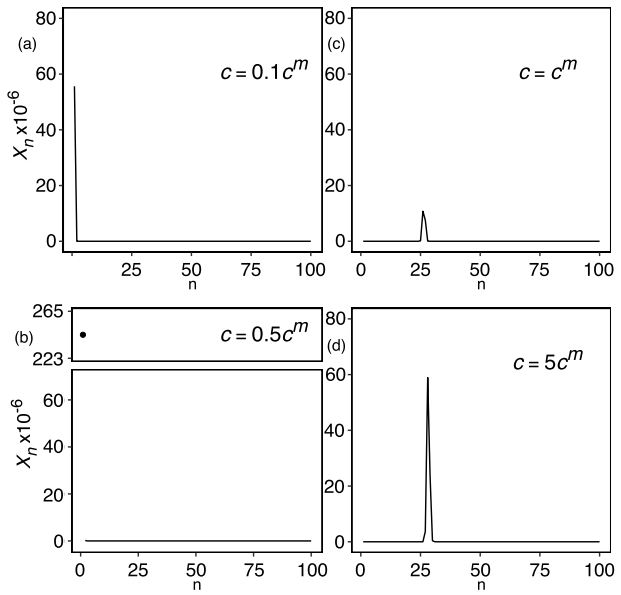

Figure 6. The micelle size distribution is shown as a function of the total concentration of AOT molecules for four values of the critical micelle concentration (c^m), defined in eq 35. The parameter α, which defines the size scaling of the ratio of activity coefficients (eq 33), was fixed to form micelles at a $c^m = 0.0049$ M.

distribution for surfactant concentration varying from less than CMC of $c = 0.1c^m$ (Figure 6a) and $c = 0.5c^m$ (Figure 6b) through $c = c^m$ (Figure 6c) to higher concentration $c = 5c^m$ (Figure 6d). The resulting micelle size distributions are narrow with width $\Delta n = 2$, which is consistent with experimental results for an AOT/alkane system.[41]

For solutions of normal micelles, it is observed that as the concentration increases near the CMC, the size distribution shows a gradual increase from monomer to normal micelle.[85] For the dry reverse micelle, we observe that surfactant AOT molecules make a sudden transition from monomer to micelle aggregate near the CMC. Such an abrupt transition from the

DOI: 10.1021/acs.jpcb.8b07847
J. Phys. Chem. B 2019, 123, 2546−2557

monomer regime to the micelle state has been anticipated but never observed in normal micelle solutions. As such, this represents a striking difference between the thermodynamics of normal micelle formation and the formation of dry RMs. The observed difference results from the magnitude of variation in $\Delta\mu_{n+1}{}^{0}$ over several kcal/mol in normal micelles and several tenths of kcal/mol in the case of dry RMs. Variations in enthalpy over tenths of a kcal/mol have been observed in an experimental study of AOT micellization in alkane solvent.[29] As the enthalpy change in surfactant AOT micellization depends on the choice of solvent, we expect a corresponding dependence of the RM size distribution on the choice of solvent.

Note that the observed transition is invariant to the specific nature of the function used to model α. Figure 7 shows the

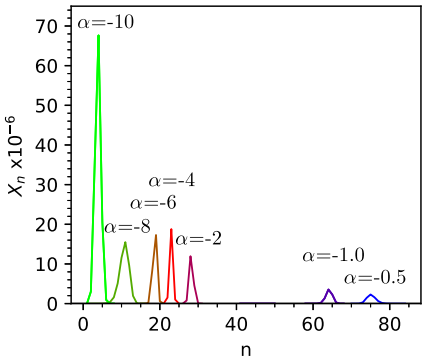

Figure 7. The aggregate size distribution for the maximum value of $\alpha(n)$ defined in eq 35. Values span a range demonstrating the regime between salt-out conditions and phase-separated conditions within which we find micellar conditions. The total concentration is fixed to be the CMC.

continuous change in the micelle size distribution as a function of α. The mean size of the dry micelle is observed to depend on the value of α, whereas the point at which AOT molecules form aggregates from monomers is relatively insensitive to α. This suggests that the sigmoidal function employed in this work to interpolate values of the activity coefficient up to the CMC, given by eq 35, does not influence the specific regime in which the first dry RM is observed.

In addition, the mean aggregate size, $\overline{n}$, for the distributions gradually increases from 1 in salt-out conditions through $\overline{n}$ = 30 by varying α from $-\infty$ to -2. This behavior is in agreement with the experimentally reported values of surfactant AOT ranging from $\overline{n}$ = 30 in *n*-octane, to 37 in *n*-decane, to $\overline{n}$ = 44 in *n*-dodecane.[40,86] This implies that if the activity coefficient only slowly increases as a function of AOT concentration, the system will display no CMC in this region. Consider the gradual increase observed in $\overline{n}$, which shows a sharp transition for 30−65 (Figure 7). Moreover, regions of higher AOT concentration may stand beyond the dilute solution limit. These specific aggregate sizes correspond to local maximum values in $\Delta\mu^{0}_{n+1}$. We must note, however, that our results for the mean free energy are accompanied by large error bars. As such, the transition from 30 to 65 may be an artifact. Assuming that the free energy surface is constant after n = 50 in $\Delta\mu^{0}_{n+1}$, our results imply that the surfactant AOT molecules become insoluble near n = 100, in agreement with the liquid crystal state of the ternary phase diagram along the AOT/isooctane line.[87]

DISCUSSION

In this study, we have obtained the size distribution of dry surfactant AOT aggregates in a nonpolar solvent. The free energy of the isolated aggregate formation was evaluated through free energy simulation using the energy representation method. The obtained free energy surface demonstrates that small surfactant aggregates can form, resulting in a dense surfactant head group region. In surfactant aggregates, the AOT heads groups disperse from the center-of-mass of the aggregate and create a core region that can accommodate isooctane solvent molecules. The spontaneous formation of a pore-like taco shell structure allows for minimization of head group repulsion and the formation of stable dry RM aggregates. In modeling the interaction of dry RM aggregates, we employed the Debye−Hückel theory scaling relation for variation in the activity coefficient with increasing aggregate number at dilute conditions. It was observed that depending on the degree of interaction, the dry RM size distribution displayed a variety of aggregate forms including soluble dry micelles and insoluble aggregates.

Previous theoretical work has doubted the existence of a CMC for dry RMs.[30,32] We believe that this was a direct result of an inability to accurately describe the free energy of solution of dry RM aggregates assuming ideal solution conditions. Recently, Kislenko and Razumov[88] investigated dry RM formation in an AOT/hexane system using thermodynamic integration and all-atom simulations. Their free energy surface showed features similar to the dependence reported here. However, their final size distribution contained dRMs of finite size, but these were found to be roughly 20 orders of magnitude smaller than that of the monomer and much lower than that of the largest aggregates which had formed due to ideal solution conditions. This demonstrates that one must account for interactions between surfactant aggregates. In this work, we obtained the formation free energy of aggregates through free energy evaluation using the energy representation method. The mean aggregate size was found to increase as a function of total surfactant concentration in a way that depends on variation in the activity coefficient.

If the activity coefficient displays a weak increase as a function of concentration, the mean aggregate size displays a gradual increase from $\overline{n}$ = 1 to 30. This dependence is determined by the variation in the chemical potential $\Delta\mu_{n+1}{}^{0}$ as a function of dry RM size. At surfactant concentrations displaying dRM sizes larger than 30, the mean aggregate size was observed to undergo an abrupt transition to much larger aggregate sizes as α (eqs 33 and 35) increases. This dependence results from the variation in the monomer activity coefficient with an increase from α = 0 (an extreme salt-out condition) to α = 1 (an ideal solution condition).

From this variation, we conclude that the interaction of surfactant aggregates in a nonpolar solvent plays a major role in dry RM formation. This behavior is quite distinct from normal micelle formation, approximately expressed using ideal solution conditions. Moreover, our results suggest why calorimetry experiments[33] have failed to observe the existence of a CMC for dry AOT surfactant RM formation.

The computed free energy surface suggests that there will be only a minor change in aggregate size distribution as a result of a modest increase in temperature of the RM phase. Note that at the threshold temperature separating the RM and liquid crystal states, intermicelle interaction is found to be a critical

DOI: 10.1021/acs.jpcb.8b07847
J. Phys. Chem. B 2019, 123, 2546−2557

point. This implies that a change in temperature cannot trigger a shift in the equilibrium state between a distribution dominated by surfactant monomers and one defined by aggregates. As such, we do not observe a maximum in the heat capacity as a function of surfactant concentration.

Our results also suggest a reason for the observed deviation in mean aggregate size in the experiment. In larger aggregates ($n > 20$), we observed the penetration of isooctane molecules in the center of the surfactant aggregate, with the solvent "core" surrounded by aliphatic tail groups of the AOT surfactant. In experimental estimates of the mean size of surfactant aggregates, it is typically assumed that the aggregate is solely composed of AOT surfactant molecules. This assumption may lead to an overestimate in the aggregation number. In the case of dry RM formation by AOT surfactant in isooctane solvent, we estimate that this overestimate of the aggregation number can be as large as 10. In addition, many experimental studies assume a spherical surfactant aggregate. However, we observe that due to the formation of the solvent core, large aggregates may deviate from a spherical shape. Moreover, the penetration of nonpolar solvents in dRMs may cause a decrease in entropy upon micellization. Additionally, it is important to note that the measurement of $\Delta\mu^0_{n+1}$ as well as these structural observations were made using results from a nonpolarizable force field. It is possible that the fixed charges in the AOT model may be too repulsive, resulting in relatively stronger carbon chain interactions that cause for the destabilization of the dRM core in these unique, nonspherical configurations at low AOT concentrations.

We compute the chemical potential in the infinite dilution limit, $\Delta\mu_{n+1}{}^0$. We have developed a theory which separates "ideal" (intramicellar) and "nonideal" (intermicellar) contributions to the free energy as dependent on surfactant concentrations which determine the dRM size distribution. The following is a brief discussion of how these contributions inform the total free energy.

Consider the reaction $R_n + A \rightleftharpoons R_{n+1}$. The equation $\mu_n = \mu_n{}^0 + kT \ln a_n = \mu_n{}^0 + kT \ln(\gamma_n X_n)$ demonstrates that the free energy consists of two terms, an ideal contribution, $\mu_n^{\text{ideal}} = \mu_n{}^0 + kT \ln X_n$ and nonideal contribution, $\mu^{\text{nonideal}} = kT \ln a_n$. The nonideal contribution can be written as $kT \ln \gamma_n = (H_n - H_n^{\text{ideal}}) - T(S_n - S_n^{\text{ideal}})$, where H_n and S_n are the enthalpy and entropy of a micelle of size n, respectively. If the size and morphology of a micelle of size $n + 1$ do not show significant change between the standard state and actual solution state, we expect that the entropic contribution to the nonideal component of $\ln(\gamma_n)$ will be modest. In contrast, the standard state enthalpic contributions from intermicelle interactions involving aggregates of size n and $n + 1$ are not expected to be significant compared to the contribution from micelle−solvent interaction. However, at higher concentration, the binding reaction is completed in the presence of other micelles. As such, the major contribution of $H_n - H_n^{\text{ideal}}$ to γ_n is due to the interaction among micelles (the interaction between micelles of size n and solvent is already included in H_n^{ideal}). No other difference exists between the chemical potential of the standard state, $\mu_n{}^0$, and the actual state, μ_n. This reasoning demonstrates that the change in activity coefficient includes contributions from intermicelle interaction as a function of AOT concentration.

We make one further observation. We have employed the chemical species model for the derivation of our thermodynamic relations. An assumption of the model is that the activity coefficient γ_n is a function of the distribution of sizes of other micelles present in the solution or that

$$\ln \gamma_n = f([\mathrm{RM}_1], [\mathrm{RM}_2], ..., [\mathrm{RM}_{n-1}], [\mathrm{RM}_{n+1}], ..., [\mathrm{RM}_{N_{\mathrm{AOT}}}]) \quad (36)$$

rather than $\ln \gamma_n = f([\mathrm{AOT}])$ which includes solute−solute interactions. On the other hand, as the total concentration of surfactant [AOT] increases, it will change the distribution of micelle sizes and the values of $[\mathrm{RM}_1]$, $[\mathrm{RM}_2]$,..., $[\mathrm{RM}_{n-1}]$, $[\mathrm{RM}_{n+1}]$,..., $[\mathrm{RM}_{N_{\mathrm{AOT}}}]$, leading to a change in the activity for each micelle size. This suggests that γ_n should vary explicitly as a function of surfactant concentration for wider regions of total [AOT]. Such strong intermicelle interaction is observed in experiments[89,90] related to mass transport and percolation in wet RMs.

Finally, the current treatment of activity in the Debye−Hückel theory is the simplest one. Although variation of the α parameter can cover the region of experimental mean aggregate size from 30 to 60, a more refined model is necessary to understand how a specific experimental condition affects the mean aggregate size. The development of a more detailed interaction model for RM formation is a future goal for the field.

In summary, our results suggest that in a nonpolar solvent, molecular interactions between surfactant aggregates and nonpolar solvent molecules play an important role in establishing equilibrium for dry RM formation due to the fact that surfactant molecules demonstrate a weak ability to associate in a nonpolar solvent. Addition of water molecules to a dry RM system leads to the formation of a wider variety of stable RMs. The extension of the formalism developed in this work to the case of wet RMs, such as those found in a ternary AOT/isooctane/water system, should allow for a similar characterization of the equilibrium RM size distribution.

AUTHOR INFORMATION

Corresponding Author

*E-mail: straub@bu.edu. Phone: (0)617.353.2500. Fax: (0) 617.353.6466.

ORCID

George A. Pantelopulos: 0000-0002-4373-1677

Notes

The authors declare no competing financial interest.

ACKNOWLEDGMENTS

We gratefully acknowledge the National Science Foundation (CHE-1362524) for the generous support of our research. G.A.P. thanks the National Science Foundation Graduate Research Fellowship Program (DGE-1247312). J.E.S. thanks the Japan Society for the Promotion of Science (JSPS) for the support provided by an Invitation Fellowship (L13523) and BRIDGE Fellowship (BR160401) hosted at Nagoya University.

REFERENCES

(1) Zhang, D.-H.; Guo, Z.; Dong, X.-Y.; Sun, Y. Characterization of lipase in reversed micelles formulated with cibacron Blue F-3GA modified Span 85. *Biotechnol. Prog.* **2007**, *23*, 108−115.

(2) Hino, T.; Kawashima, Y.; Shimabayashi, S. Basic study for stabilization of w/o/w emulsion and its application to transcatheter

DOI: 10.1021/acs.jpcb.8b07847
J. Phys. Chem. B 2019, 123, 2546−2557

arterial embolization therapy. *Adv. Drug Delivery Rev.* **2000**, *45*, 27−45.
(3) Okochi, H.; Nakano, M. Preparation and evaluation of w/o/w type emulsions containing vancomycin. *Adv. Drug Delivery Rev.* **2000**, *45*, 5−26.
(4) Higashi, S.; Setoguchi, T. Hepatic arterial injection chemotherapy for hepatocellular carcinoma with epirubicin aqueous solution as numerous vesicles in iodinated poppy-seed oil microdroplets: clinical application of water-in-oil-in-water emulsion prepared using a membrane emulsification technique. *Adv. Drug Delivery Rev.* **2000**, *45*, 57−64.
(5) Nishii, Y.; Kinugasa, T.; Nii, S.; Takahashi, K. Transport behavior of protein in bulk liquid membrane using reversed micelles. *J. Membr. Sci.* **2002**, *195*, 11−21.
(6) Nucci, N. V.; Valentine, K. G.; Wand, A. J. High-resolution NMR spectroscopy of encapsulated proteins dissolved in low-viscosity fluids. *J. Magn. Reson.* **2014**, *241*, 137−147.
(7) Dodevski, I.; Nucci, N. V.; Valentine, K. G.; Sidhu, G. K.; O'Brien, E. S.; Pardi, A.; Wand, A. J. Optimized reverse micelle surfactant system for high-resolution NMR spectroscopy of encapsulated proteins and nucleic acids dissolved in low viscosity fluids. *J. Am. Chem. Soc.* **2014**, *136*, 3465−3474.
(8) Karsa, D. R. *Industrial Applications of Surfactants IV*; The Royal Society of Chemistry: London, 1999.
(9) Schramm, L. L. *Surfactants: Fundamentals and Applications in the Petroleum Industry*; Cambridge University Press: Cambridge, 2000.
(10) Rosen, M. J., Kunjappu, J. T. *Surfactants and Interfacial Phenomena*; John Wiley & Sons: Hoboken, 2012.
(11) Galamba, N. Water's structure around hydrophobic solutes and the iceberg model. *J. Phys. Chem. B* **2013**, *117*, 2153−2159.
(12) Galamba, N. Water tetrahedrons, hydrogen-bond dynamics, and the orientational mobility of water around hydrophobic solutes. *J. Phys. Chem. B* **2014**, *118*, 4169−4176.
(13) Schick, M. J. *Nonionic Surfactants: Physical Chemistry*; Marcel Dekker: New York, 1987.
(14) Aranow, R. H.; Witten, L. The environmental influence on the behavior of long chain molecules[1]. *J. Phys. Chem.* **1960**, *64*, 1643−1648.
(15) Aranow, R. H.; Witten, L. Additional comments on the thermodynamics of environmental changes of the methylene group. *J. Chem. Phys.* **1965**, *43*, 1436−1437.
(16) Shiraga, K.; Suzuki, T.; Kondo, N.; Ogawa, Y. Hydration and hydrogen bond network of water around hydrophobic surface investigated by terahertz spectroscopy. *J. Chem. Phys.* **2014**, *141*, No. 235103.
(17) Frank, H. S.; Evans, M. W. Free volume and entropy in condensed systems III. entropy in binary liquid mixtures; partial molal entropy in dilute solutions; structure and thermodynamics in aqueous electrolytes. *J. Chem. Phys.* **1945**, *13*, 507−532.
(18) Eicke, H.-F.; Christen, H. Is water critical to the formation of micelles in apolar media?? *Helv. Chim. Acta* **1978**, *61*, 2258−2263.
(19) Van Dijk, M. A.; Joosten, J. G. H.; Levine, Y. K.; Bedeaux, D. Dielectric study of temperature-dependent aerosol OT/water/isooctane microemulsion structure. *J. Phys. Chem.* **1989**, *93*, 2506−2512.
(20) Fathi, H.; Kelly, J. P.; Vasquez, V. R.; Graeve, O. A. Ionic concentration effects on reverse micelle size and stability: Implications for the synthesis of nanoparticles. *Langmuir* **2012**, *28*, 9267−9274.
(21) Chowdhary, J.; Ladanyi, B. M. Molecular dynamics simulation of Aerosol-OT reverse micelles. *J. Phys. Chem. B* **2009**, *113*, 15029−15039.
(22) Eskici, G.; Axelsen, P. H. The size of AOT reverse micelles. *J. Phys. Chem. B* **2016**, *120*, 11337−11347.
(23) Faeder, J.; Ladanyi, B. M. Molecular dynamics simulations of the interior of aqueous reverse micelles. *J. Phys. Chem. B* **2000**, *104*, 1033−1046.
(24) Faeder, J.; Ladanyi, B. M. Solvation dynamics in aqueous reverse micelles:? A computer simulation study. *J. Phys. Chem. B* **2001**, *105*, 11148−11158.
(25) Chowdhary, J.; Ladanyi, B. M. Molecular simulation study of water mobility in Aerosol-OT reverse micelles. *J. Phys. Chem. A* **2011**, *115*, 6306−6316.
(26) Graeve, O. A.; Fathi, H.; Kelly, J. P.; Saterlie, M. S.; Sinha, K.; Rojas-George, G.; Kanakala, R.; Brown, D. R.; Lopez, E. A. Reverse micelle synthesis of oxide nanopowders: Mechanisms of precipitate formation and agglomeration effects. *J. Colloid Interface Sci.* **2013**, *407*, 302−309.
(27) Mukherjee, S.; Chowdhury, P.; Gai, F. Tuning the cooperativity of the helix-coil transition by aqueous reverse micelles. *J. Phys. Chem. B* **2006**, *110*, 11615−11619.
(28) Mukherjee, S.; Chowdhury, P.; DeGrado, W. F.; Gai, F. Site-specific hydration status of an amphipathic peptide in AOT reverse micelles. *Langmuir* **2007**, *23*, 11174−11179.
(29) Mukherjee, K.; Moulik, S.; Mukherjee, D. Thermodynamics of micellization of Aerosol OT in polar and nonpolar solvents. A calorimetric study. *Langmuir* **1993**, *9*, 1727−1730.
(30) Ruckenstein, E.; Nagarajan, R. Aggregation of amphiphiles in nonaqueous media. *J. Phys. Chem.* **1980**, *84*, 1349−1358.
(31) Ekwall, P.; Mandell, L.; Fontell, K. Some observations on binary and ternary aerosol OT systems. *J. Colloid Interface Sci.* **1970**, *33*, 215−235.
(32) Wootton, A.; Picavez, F.; Harrowell, P. The structure and thermodynamic stability of reverse micelles in dry AOT/Alkane Mixtures. *AIP Conf. Proc.* **2008**, *982*, 289−294.
(33) Tanaka, R. Calorimetric studies of micellar formation of amphiphiles in nonaqueous solutions. *J. Jpn. Oil Chem. Soc.* **1992**, *41*, 82−90.
(34) Tanaka, R.; Yokoyama, T.; Sameshima, K.; Kawase, T. Growth of AOT reversed micelles and the solvent effect investigated by dielectric and light-scattering measurements. *Bull. Chem. Soc. Jpn.* **2005**, *78*, 599−603.
(35) Sameshima, K.; Tanaka, R.; Igarashi, K.; Ooshima, H. Studies on the hydration of Aerosol OT and the formation of reversed micelles in decane by a calorimetry and ab initio calculations. *J. Chem. Thermodyn.* **2006**, *38*, 662−671.
(36) Chen, S. H. Small angle neutron scattering studies of the structure and interaction in micellar and microemulsion systems. *Annu. Rev. Phys. Chem.* **1986**, *37*, 351−399.
(37) Muto, S.; Meguro, K. The determination of the CMC of surfactants in some organic solvents. *Bull. Chem. Soc. Jpn.* **1973**, *46*, 1316−1320.
(38) Kon-no, K.; Kitahara, A. Micelle formation of oil-soluble surfactants in nonaqueous solutions: Effect of molecular structure of surfactants. *J. Colloid Interface Sci.* **1971**, *35*, 636−642.
(39) Kitahara, A.; Kobayashi, T.; Tachibana, T. Light scattering study of solvent effect on micelle formation of Aersol OT[1]. *J. Phys. Chem.* **1962**, *66*, 363−365.
(40) Frank, S. G.; Zografi, G. Determination of micellar weights for di-alkyl sodium sulfosuccinates in anhydrous and hydrous hydrocarbon solutions. *J. Pharm. Sci.* **1969**, *58*, 993−997.
(41) Smith, G. N.; Brown, P.; Rogers, S. E.; Eastoe, J. Evidence for a critical micelle concentration of surfactants in hydrocarbon solvents. *Langmuir* **2013**, *29*, 3252−3258.
(42) Smith, G. N.; Brown, P.; James, C.; Rogers, S. E.; Eastoe, J. The effect of solvent and counterion variation on inverse micelle CMCs in hydrocarbon solvents. *Colloids Surf., A* **2016**, *494*, 194−200.
(43) Hollamby, M. J.; Tabor, R.; Mutch, K. J.; Trickett, K.; Eastoe, J.; Heenan, R. K.; Grillo, I. Effect of solvent quality on aggregate structures of common surfactants. *Langmuir* **2008**, *24*, 12235−12240.
(44) Christopher, P.; Oxtoby, D. W. Free energy and size distributions of micelles in solution. *J. Chem. Phys.* **2003**, *118*, 5665−5672.
(45) Mohan, G.; Kopelevich, D. I. A multiscale model for kinetics of formation and disintegration of spherical micelles. *J. Chem. Phys.* **2008**, *128*, No. 044905.
(46) Kindt, J. T. Accounting for finite-number effects on cluster size distributions in simulations of equilibrium aggregation. *J. Chem. Theory Comput.* **2013**, *9*, 147−152.

DOI: 10.1021/acs.jpcb.8b07847
J. Phys. Chem. B 2019, 123, 2546−2557

(47) Ben-Shaul, A.; Gelbart, W. M. Effect of interaggregate forces on the size distribution of micelles. *J. Phys. Chem.* **1982**, *86*, 316−318.
(48) Kinoshita, M.; Sugai, Y. A new methodology for predicting shape and size distribution of micelles. *Chem. Phys. Lett.* **1999**, *313*, 685−692.
(49) Kinoshita, M.; Sugai, Y. Methodology of predicting approximate shapes and size distribution of micelles: illustration for simple models. *J. Comput. Chem.* **2002**, *23*, 1445−1455.
(50) Yoshii, N.; Okazaki, S. A molecular dynamics study of structural stability of spherical SDS micelle as a function of its size. *Chem. Phys. Lett.* **2006**, *425*, 58−61.
(51) Yoshii, N.; Okazaki, S. A molecular dynamics study of surface structure of spherical SDS micelles. *Chem. Phys, Lett.* **2006**, *426*, 66−70.
(52) Yoshii, N.; Iwahashi, K.; Okazaki, S. A molecular dynamics study of free energy of micelle formation for sodium dodecyl sulfate in water and its size distribution. *J. Chem. Phys.* **2006**, *124*, No. 184901.
(53) Yoshii, N.; Okazaki, S. A molecular dynamics study of structure and dynamics of surfactant molecules in SDS spherical micelle. *Condens. Matter Phys.* **2007**, *10*, 573−578.
(54) Matubayasi, N.; Nakahara, M. Theory of solutions in the energetic representation. I. Formulation. *J. Chem. Phys.* **2000**, *113*, 6070.
(55) Matubayasi, N.; Nakahara, M. Theory of solutions in the energy representation. II. Functional for the chemical potential. *J. Chem. Phys.* **2002**, *117*, 3605.
(56) Matubayasi, N.; Nakahara, M. Theory of solutions in the energy representation. III. Treatment of the molecular flexibility. *J. Chem. Phys.* **2003**, *119*, 9686.
(57) Tanford, C. *The Hydrophobic Effect: Formation of Micelles and Biological Membranes*, 2nd ed.; Wiley: New York, 1980.
(58) Puvvada, S.; Blankschtein, D. Molecular-thermodynamic approach to predict micellization, phase behavior and phase separation of micellar solutions. I. Application to nonionic surfactants. *J. Chem. Phys.* **1990**, *92*, 3710−3724.
(59) Zoeller, N.; Lue, L.; Blankschtein, D. Statistical-thermodynamic framework to model nonionic micellar solutions. *Langmuir* **1997**, *13*, 5258−5275.
(60) Kindt, J. T. personal communication.
(61) Frolov, A. I. Accurate calculation of solvation free energies in supercritical fluids by fully atomistic simulations: Probing the theory of solutions in energy representation. *J. Chem. Theory Comput.* **2015**, *11*, 2245−2256.
(62) Sakuraba, S.; Matubayasi, N. Ermod: Fast and versatile computation software for solvation free energy with approximate theory of solutions. *J. Comput. Chem.* **2014**, *35*, 1592−1608.
(63) Martínez, L.; Andrade, R.; Birgin, E. G.; Martínez, J. M. PACKMOL: A package for building initial configurations for molecular dynamics simulations. *J. Comput. Chem.* **2009**, *30*, 2157−2164.
(64) Abel, S.; Sterpone, F.; Bandyopadhyay, S.; Marchi, M. Molecular modeling and simulations of AOT-water reverse micelles in isooctane: structural and dynamic properties. *J. Phys. Chem. B* **2004**, *108*, 19458−19466.
(65) Humphrey, W.; Dalke, A.; Schulten, K. VMD: Visual molecular dynamics. *J. Mol. Graph.* **1996**, *14*, 33−38.
(66) Berendsen, H.; van der Spoel, D.; van Drunen, R. GROMACS: A message-passing parallel molecular dynamics implementation. *Comput. Phys. Commun.* **1995**, *91*, 43−56.
(67) Páll, S.; Abraham, M. J.; Kutzner, C.; Hess, B.; Lindahl, E. In *Tackling Exascale Software Challenges in Molecular Dynamics Simulations with GROMACS*, International Conference on Exascale Applications and Software; Markidis, S., Laure, E., Eds.; Springer International Publishing, 2015; pp 3−27.
(68) Abraham, M. J.; Murtola, T.; Schulz, R.; Páll, S.; Smith, J. C.; Hess, B.; Lindahl, E. GROMACS: High performance molecular simulations through multi-level parallelism from laptops to supercomputers. *SoftwareX* **2015**, *1−2*, 19−25.
(69) R Core Team, R. *A Language and Environment for Statistical Computing*, version 3.2.0; R Foundation for Statistical Computing: Vienna, Austria, 2015.
(70) Ihaka, R.; Gentleman, R. R: A language for data analysis and graphics. *J. Comput. Graph. Stat.* **1996**, *5*, 299−314.
(71) Adler, D.; Murdoch, D. et al. *rgl: 3D Visualization using OpenGL*, R package version 0.95.1441, 2016.
(72) Nave, S.; Eastoe, J.; Penfold, J. What is so special about Aerosol-OT? 1. Aqueous systems. *Langmuir* **2000**, *16*, 8733−8740.
(73) Martin, C. A.; Magid, L. J. Carbon-13 NMR investigations of Aerosol OT water/oil microemulsions. *J. Phys. Chem.* **1981**, *85*, 3938−3944.
(74) Hsu, M. F.; Dufresne, E. R.; Weitz, D. A. Charge stabilization in nonpolar solvents. *Langmuir* **2005**, *21*, 4881−4887.
(75) Briscoe, W. H.; Horn, R. G. Direct measurement of surface forces due to charging of solids immersed in a nonpolar liquid. *Langmuir* **2002**, *18*, 3945−3956.
(76) Hsu, M. F.; Dufresne, E. R.; Weitz, D. A. Charge stabilization in nonpolar solvents. *Langmuir* **2005**, *21*, 4881−4887.
(77) Piñero, J.; Bhuiyan, L.; Bratko, D. Electrostatic interactions of charged dipolar proteins in reverse micelles. *J. Chem. Phys.* **2004**, *120*, 11941−11947.
(78) Roberts, G. S.; Sanchez, R.; Kemp, R.; Wood, T.; Bartlett, P. Electrostatic charging of nonpolar colloids by reverse micelles. *Langmuir* **2008**, *24*, 6530−6541.
(79) Sainis, S. K.; Germain, V.; Mejean, C. O.; Dufresne, E. R. Electrostatic interactions of colloidal particles in nonpolar solvents: Role of surface chemistry and charge control agents. *Langmuir* **2008**, *24*, 1160−1164.
(80) Eicke, H. F.; Borkovec, M.; Das-Gupta, B. Conductivity of water-in-oil microemulsions: a quantitative charge fluctuation model. *J. Phys. Chem.* **1989**, *93*, 314−317.
(81) De, T. K.; Maitra, A. Solution behaviour of Aerosol OT in nonpolar solvents. *Adv. Colloid Interface Sci.* **1995**, *59*, 95−193.
(82) Mathew, C.; Patanjali, P. K.; Nabi, A.; Maitra, A. On the concept of percolative conduction in water-in-oil microemulsions. *Colloids Surf.* **1988**, *30*, 253−263.
(83) Grest, G. S.; Webman, I.; Safran, S. A.; Bug, A. L. R. Dynamic percolation in microemulsions. *Phys. Rev. A* **1986**, *33*, 2842−2845.
(84) Huang, J. S.; Safran, S. A.; Kim, M. W.; Grest, G. S.; Kotlarchyk, M.; Quirke, N. Attractive Interactions in Micelles and Microemulsions. *Phys. Rev. Lett.* **1984**, *53*, 592−595.
(85) Diamant, H.; Andelman, D. Free energy approach to micellization and aggregation: Equilibrium, metastability, and kinetics. *Curr. Opin. Colloid Interface Sci.* **2016**, *22*, 94−98.
(86) Eicke, H. F. Surfactants in nonpolar solvents. Aggregation and micellization. *Top. Curr. Chem.* **1980**, *87*, 85.
(87) Tamamushi, B.; Watanabe, N. The formation of molecular aggregation structures in ternary system: Aerosol OT/water/isooctane. *Colloid Polym. Sci.* **1980**, *258*, 174−178.
(88) Kislenko, S.; Razumov, V. Molecular dynamics study of micellization thermodynamics in AOT/hexane system. *Colloid J.* **2017**, *79*, 76−80.
(89) Fletcher, P. D.; Howe, A. M.; Robinson, B. H. The kinetics of solubilisate exchange between water droplets of a water-in-oil microemulsion. *J. Chem. Soc., Faraday Trans. 1* **1987**, *83*, 985−1006.
(90) Mejuto, J.; Morales, J.; Moldes, O.; Cid, A. Effects of additives upon percolation temperature in AOT-based microemulsions. *J. Appl. Solution Chem. Model.* **2014**, *3*, 106−129.

DOI: 10.1021/acs.jpcb.8b07847
J. Phys. Chem. B 2019, 123, 2546−2557